
AFRL-RZ-WP-TP-2010-2050

# INK-JET PRINTING: A VERSATILE METHOD FOR MULTILAYER SOLID OXIDE FUEL CELLS FABRICATION (POSTPRINT)

**Thomas L. Reitz and Ryan M. Miller**

**Thermal & Electrochemical Branch**
**Energy/Power/Thermal Division**

**Mary A. Sukeshini and Ryan Cummins**

**Wright State University**

**FEBRUARY 2010**



**AIR FORCE RESEARCH LABORATORY**
**PROPULSION DIRECTORATE**
**WRIGHT-PATTERSON AIR FORCE BASE, OH 45433-7251**
**AIR FORCE MATERIEL COMMAND**
**UNITED STATES AIR FORCE**

# REPORT DOCUMENTATION PAGE

*Form Approved*
*OMB No. 0704-0188*



| 1. REPORT DATE *(DD-MM-YY)* | 2. REPORT TYPE | 3. DATES COVERED *(From - To)* |
|---|---|---|
| February 2010 | Journal Article Postprint | 01 January 2009 – 01 April 2009 |

**4. TITLE AND SUBTITLE**
INK-JET PRINTING: A VERSATILE METHOD FOR MULTILAYER SOLID OXIDE FUEL CELLS FABRICATION (POSTPRINT)

**5a. CONTRACT NUMBER**
In-house

**5b. GRANT NUMBER**

**5c. PROGRAM ELEMENT NUMBER**
62203F

**6. AUTHOR(S)**
Thomas L. Reitz and Ryan M. Miller (AFRL/RZPS)
Mary A. Sukeshini and Ryan Cummins (Wright State University)

**5d. PROJECT NUMBER**
3145

**5e. TASK NUMBER**
01

**5f. WORK UNIT NUMBER**
314501CK

**7. PERFORMING ORGANIZATION NAME(S) AND ADDRESS(ES)**
Thermal & Electrochemical Branch (AFRL/RZPS)
Energy/Power/Thermal Division
Air Force Research Laboratory, Propulsion Directorate
Wright-Patterson Air Force Base, OH 45433-7251
Air Force Materiel Command, United States Air Force

Wright State University
Department of Mechanical and Materials Engineering
Dayton, OH 45430

**8. PERFORMING ORGANIZATION REPORT NUMBER**
AFRL-RZ-WP-TP-2010-2050

**9. SPONSORING/MONITORING AGENCY NAME(S) AND ADDRESS(ES)**
Air Force Research Laboratory
Propulsion Directorate
Wright-Patterson Air Force Base, OH 45433-7251
Air Force Materiel Command
United States Air Force

**10. SPONSORING/MONITORING AGENCY ACRONYM(S)**
AFRL/RZPS

**11. SPONSORING/MONITORING AGENCY REPORT NUMBER(S)**
AFRL-RZ-WP-TP-2010-2050

**12. DISTRIBUTION/AVAILABILITY STATEMENT**
Approved for public release; distribution unlimited.

**13. SUPPLEMENTARY NOTES**
Journal article published in *J. Am. Ceram. Soc.*, Vol. 92, No. 12, 2009. PA Case Number: 88ABW-2009-1340; Clearance Date: 06 April 2009. Paper contains color. 

**14. ABSTRACT**
The potential of ink-jet printing for fabrication of components for solid oxide fuel cells has been explored. An anode interlayer, consisting of a composite of NiO and yttria-stabilized zirconia (YSZ), and an electrolyte layer, YSZ (8 mol%), were ink-jet printed on a tape cast anode support, 55 wt% NiO–45 wt% YSZ (8 mol%). Scanning electron microscopy of the printed layers sintered at 1400°C revealed a dense electrolyte layer measuring 10–12 μm in thickness. Single cells using these printed layers and strontium-doped lanthanum manganate (LSM, $La_{0.8}Sr_{0.2}MnO_3$)-based pasted cathodes were assessed by DC polarization and AC complex impedance methods. The cells exhibited a stable open circuit voltage of 1.1 V around 800°C, in a hydrogen atmosphere. A maximum power density of 500 $m \cdot (W \cdot cm)^{-2}$ was achieved at 850°C for a typical cell with the electrolyte and anode interlayer cosintered at 1400°C. A composite cathode interlayer, LSM–YSZ, and a cathode current collection layer, LSM, were also ink-jet printed and incorporated in single cells. However, cells with all components ink-jet printed showed decreased performance. This pointed to critical issues in the composite cathode microstructure, which is controlled by the composite ink design/formulation and printing parameters that need to be addressed.

**15. SUBJECT TERMS**
solid oxide fuel cell, ink jet printing

| 16. SECURITY CLASSIFICATION OF: | | | 17. LIMITATION OF ABSTRACT: | 18. NUMBER OF PAGES | 19a. NAME OF RESPONSIBLE PERSON (Monitor) |
|---|---|---|---|---|---|
| a. REPORT | b. ABSTRACT | c. THIS PAGE | | | Stanley Rodrigues |
| Unclassified | Unclassified | Unclassified | SAR | 14 | 19b. TELEPHONE NUMBER *(Include Area Code)* N/A |

**Standard Form 298 (Rev. 8-98)**
Prescribed by ANSI Std. Z39-18

journal

J. Am. Ceram. Soc., 92 [12] 2913–2919 (2009)
DOI: 10.1111/j.1551-2916.2009.03349.x


# Ink-Jet Printing: A Versatile Method for Multilayer Solid Oxide Fuel Cells Fabrication

Mary A. Sukeshini*,† and Ryan Cummins

Department of Mechanical and Materials Engineering, Wright State University, Dayton, Ohio 45430

Thomas L. Reitz and Ryan M. Miller

The Air Force Research Laboratory, Propulsion Directorate, Wright-Patterson Air Force Base, Ohio 45433

**The potential of ink-jet printing for fabrication of components for solid oxide fuel cells has been explored. An anode interlayer, consisting of a composite of NiO and yttria-stabilized zirconia (YSZ), and an electrolyte layer, YSZ (8 mol%), were ink-jet printed on a tape cast anode support, 55 wt% NiO–45 wt% YSZ (8 mol%). Scanning electron microscopy of the printed layers sintered at 1400°C revealed a dense electrolyte layer measuring 10–12 μm in thickness. Single cells using these printed layers and strontium-doped lanthanum manganate (LSM, $La_{0.8}Sr_{0.2}MnO_3$)-based pasted cathodes were assessed by DC polarization and AC complex impedance methods. The cells exhibited a stable open circuit voltage of 1.1 V around 800°C, in a hydrogen atmosphere. A maximum power density of 500 $m \cdot (W \cdot cm)^{-2}$ was achieved at 850°C for a typical cell with the electrolyte and anode interlayer cosintered at 1400°C. A composite cathode interlayer, LSM–YSZ, and a cathode current collection layer, LSM, were also ink-jet printed and incorporated in single cells. However, cells with all components ink-jet printed showed decreased performance. This pointed to critical issues in the composite cathode microstructure, which is controlled by the composite ink design/formulation and printing parameters that need to be addressed.**

## I. Introduction

Solid oxide fuel cells (SOFCs) have attracted considerable interest owing to their potential for clean and efficient power generation, fuel flexibility, and other benefits such as ability to use high-temperature exhaust for cogeneration.[1,2] A typical yttria-stabilized zirconia (YSZ) electrolyte-based SOFC operates at 800°–1000°C and consists of both bulk and thick-film components. One of the factors that limit the commercialization of SOFC's is the need for high-operating temperatures due to the materials involved and fabrication processes that are not cost effective. To address these concerns, researchers are actively exploring thinner electrolytes to compensate for ohmic loss at intermediate operating temperatures and highly electro-catalytically active electrode materials to balance slower electrode kinetics.[3,4] Multilayered cell configurations are becoming increasingly popular as these designs enable a combination of properties that are both mechanically and electrochemically superior.[5,6] Typically these thin intermediate electrode layers have specific functionality of either extending the electrochemically active triple phase boundary into the bulk of the electrode[7,8] or serving as barrier layers to avoid deleterious reactions between components.[9] They also function as layers that bridge the difference between the thermal coefficient of expansion between components.[10] More recently, cells with complex geometries, including segmented in-series SOFCs, have been shown to have high-power densities comparable to planar cells. These cells require precise positioning of overlapping multiple layers.[11,12] To achieve these thin films with carefully controlled thicknesses in order to achieve optimal cell performance in multilayered cells, a number of fabrication methods based on chemical routes (chemical vapor deposition, electrochemical vapor deposition, sol–gel based, and spray pyrolisis), physical routes (rf magnetron sputtering, thermal spray, and pulsed laser deposition), and conventional ceramic methods (screen-printing, tape casting, slurry coating, slip casting, tape calendaring, and electrophoretic deposition) are being used.[13–18] Methods based on physical vapor deposition involve high equipment costs and are difficult to scale up. The more commonly used methods for thick-film deposition through colloidal preparations of tape casting, slurry, and dip coating are relatively easy to set up and scale but film uniformity and accurate control of thickness from batch to batch remain a challenge.

Ink-jet printing, which has been traditionally used in the commercially mature realm of reprography, is now being explored as a viable method for deposition of thin layers in diverse areas including electronics processing, ceramics, and biological culture research.[19–25] This method has the potential to be extended to SOFC fabrication. Some attractive features of ink-jet printing are simplicity, accurate control of features by computer-aided design and automation, and ease of mass manufacture. Being an additive method, ink-jet printing allows maskless deposition of materials in desired patterns without the need for complex processing. With accurate $x$–$y$ spatial control, a high level of reproducibility can be expected, a feature lacking in competing approaches for SOFC fabrication such as tape casting, spray, and dip coating. It is only very recently that ink-jet printing has received the attention of researchers for application in SOFC's.[26,27] In our previous study,[26] we demonstrated the fabrication of single SOFCs, where the anode interlayer and electrolyte layers were ink-jet printed. While the printed layers (YSZ and NiO–YSZ) were seen to be dense and porous, respectively, the performance and stability of cells fabricated left much to be desired. While a good cell voltage was observed, the performance of the cell was not satisfactory and was not stable at temperatures $>700°$–750°C. Problems relating to integration of printed layers with the anode support due to poor overall microstructure of the cell were observed. Differences in particle size in the anode functional layer ink, type of anode support, and processing parameters appeared to impact the cell integrity and behavior. Furthermore, a clear determination of the cause of poor performance was not possible because of the preliminary nature of the work. In this work, we have circumvented such issues and have attempted to ink-jet print a complete cell

W.-C. Wei—contributing editor

Manuscript No. 26117. Received April 17, 2009; approved July 29, 2009.
This paper was presented in part at the "33rd International conference and exposition on advanced ceramics and composites: 6th International symposium on solid oxide fuel cell, Daytona Beach, FL, January 18–23, 2009 (Abstract book, 127pp.)."
*Member, The American Ceramic Society.
†Author to whom correspondence should be addressed. e-mail: mary.ayyadurai.ctr@wpafb.af.mil

incorporating an anode functional layer, electrolyte, cathode functional layer, and cathode current collection layer. It is envisioned that through this work we will not only demonstrate the applicability of ink-jet approach to SOFC production but also establish the feasibility of this approach for other ceramic thin-film devices such as dielectric capacitors.

## II. Experimental Procedure

### (1) Ink Preparation and Rheology

In order to prepare suitable electrolyte and anode-interlayer inks, commercial sources of ceramic materials were selected. YSZ (8 mol %, TZ-8YS, Tosoh Co., Tokyo, Japan) was used for both the electrolyte and the anode functional layers. NiO powder, (0.2–0.4 μm, NexTech, Columbus, OH) and TZ-8YS mixture in a 50–50 wt% was used for the anode interlayer inks. For the cathode interlayer ink, strontium-doped lanthanum manganate (LSM, $La_{0.8}Sr_{0.2}MnO_3$, 7.827 $m^2/g$, NexTech) and TZ-8YS was used. LSM powder was used in the ink for the cathode current collector layer. α-Terpineol was used as the solvent for the ink slurries. Polyvinyl butyral (PVB), butyl benzyl phthalate (BBP), and polyalkalyne glycol (PAG) were utilized as binder and plasticizer constituents. All inks were prepared by simultaneous addition of powders, binder, and plasticizers to α-terpineol followed by >12 h of ball milling with 5-mm-diameter YSZ beads in a glass container. The composition of solids used in the ink for the electrolyte, anode/cathode functional layer, and cathode current collector is shown in Table I. Viscosity measurements for the various ink formulations were obtained using a Rheolab QC (Anton-Paar, Ashland, VA) rheometer.

### (2) Printing/Cell Fabrication, Electrochemical Measurements, and Microstructure

Printing of layers was carried out using the DIMATIX DMP 2831 ink-jet printer (FujiFilm, Santa Clara, CA). The firing segment of the driving waveform was characterized by a jetting amplitude of 32 V, and a 2.944 μs pulse width with a slew rate of 0.93 V/μs at a frequency of 3 kHz. This jetting profile was used for printing all layers, including the anode interlayer, electrolyte, cathode interlayer, and cathode current collection layer. Each layer was typically produced through multiple passes in succession, with the ink-jet head operating at a temperature above ambient. The choice of the ink-jet head/cartridge temperature was dictated by the different drying rates of printed layers with composite versus single component precursors. Details are presented in the following sections.

*(A) Anode Interlayer and Electrolyte:* The anode support used as a substrate consisted of a commercially supplied sample made from a isostatically laminated green tape (55 wt% NiO/45 wt% YSZ, ESL Electroscience, King of Prussia, PA). These anode supports were prepared with two different types of carbon pore formers; plate-like (type-A), and granule (type-B). After initial testing, type-B supports were used for subsequent studies. The support was initially bisque fired at 950°C in order to drive off solvent, as well as impart mechanical integrity. A total of 10 passes of the anode interlayer were printed over this support using the anode interlayer ink, followed by a second bisque firing at 950°C. The internal cartridge temperature was set to 58°C and the platen temperature was kept at 80°C at the end of printing to enable drying of the printed layers. A total of 12 passes of electrolyte were printed over the anode interlayer using the electrolyte ink in a similar manner. For this layer, the internal cartridge temperature was set to 48°C. The anode/anode interlayer/electrolyte structure was then cofired at 1400°C for 2 h.

*(B) Cathode Interlayer and Cathode Current Collection Layer:* Two sets of cells were fabricated depending on the type of cathode layers. Cells composed of printed anode interlayer and electrolyte layers but with pasted cathode layers are designated "PS" while those prepared entirely through printing are designated "PR." For PS cells, the cathode interlayer and cathode current collector layers were hand pasted from a thick ink paste. For the cathode interlayer paste, 22.5 wt% of LSM and 22.5 wt% of YSZ powders were mixed together and ball milled. This mixture was added to a sonicated mixture of solvents containing 13.5 wt% of xylene, 13.5 wt% of ethanol, 16.2 wt% of terpineol, and 1.1 wt% of fish oil, and ball milled overnight. 5.6 wt% of PVB, 0.5 wt% of BBP, and 4.5 wt% of PAG were added to the slurry and again ball milled overnight. The resulting paste was then hand painted over the printed electrolyte. The coupon was then sintered at 1200°C for 1 h. Finally, a cathode current collection layer was hand painted using a pure LSM paste (LSM paste, NexTech) and sintered at 1200°C. "PR" cells were fabricated to explore the possibility of printing the cathode interlayer and cathode current collection layers in addition to the anode interlayer and electrolyte. For these cells, the cathode layers (interlayer and current collectors) were ink-jet printed. Printed cathode interlayer films were prepared with 20 successive passes of the cathode interlayer ink on a circular area over the electrolyte. Internal cartridge temperature for printing was 58°C. The platen temperature was maintained at 100°C for drying of the deposited layer. Cathode current collector layers were prepared by 30 successive passes of the pure LSM ink over the cathode interlayer. Internal cartridge temperature for printing was 48°C. For the deposition of the cathode layers (cathode interlayer as well as the cathode current collection layer), the platen (substrate) temperature for drying was observed to be critical. If the temperature was too low (40°–70°C), the ink was seen to flow and spread beyond the preset circular print area. If it was too high, distinct "coffee ring" (drop with different thickness at the edge compared with the center) patterns were visible on inspection of the printed layer under an optical microscope. The optimum temperature (100°C in the present case) keeps the drying front approximately 1/8 in. behind the print head and allows drying such that the deposition does not spread beyond the preset print area with diameter of 13 mm.

All sintering steps were identical to the pasted cathode cells. The area defined by 13 mm diameter of the cathode interlayer/cathode current collection layer was considered as the active area for the cell and used as the basis for calculation of current density.

*(C) Cell Assembly, Electrochemical Testing, and Post-Testing Microstructure Study:* Silver leads were attached on the cathode and anode sides using gold paste. The cells were then glued onto one end of a ceramic tube using a ceramic paste (Ultratemp 516, Aremco, Valley Cottage, NY) and housed in a tube furnace. During characterization of each cell, the furnace was slowly heated to desired temperatures (up to 850°C) for electrochemical characterization. The anode side was reduced in forming gas (5% hydrogen in argon), while the cathode side was exposed to forced air. After reducing for several hours, the anode side was exposed to dry hydrogen at a flow rate of 65 sccm.

The cell performance and electrochemical impedance spectra were measured using a multichannel electrochemical test station comprised of a Solartron 1470E potentiostat/galvanostat combined with a Solartron 1450 frequency response analyzer (Solartron Analytical, U.K.). Impedance spectroscopy measurements were obtained in potentiostatic mode, under open circuit conditions, over a frequency range of 1 MHz–50 mHz. For the impedance measurements, the excitation amplitude remained fixed at 10 mV. After electrochemical testing, the cells were cooled to room temperature with the anode side exposed to a reducing atmosphere of forming gas. After cooling, the morphology and microstructure were characterized using a JEOL JSM7401-F field-emission scanning electron microscope (Jeol, Germany).

## III. Results and Discussion

### (1) Ink Rheology and Shelf Life

In order to sustain stable ink formulations, solids loading was kept low (see Table I) resulting in low-viscosity formulations. In

**Table I. Ink Compositions**

| Constituent | Anode interlayer (wt%) | Electrolyte (wt%) | Cathode interlayer (wt%) | Cathode current collector layer (wt%) |
|---|---|---|---|---|
| α-Terpineol | 94.1 | 89 | 96.8 | 89 |
| YSZ | 2.8 | 10.7 | 1.45 | 0 |
| NiO | 2.8 | 0 | 0 | 0 |
| LSM | 0 | 0 | 1.45 | 10.7 |
| PAG | 0.1 | 0.1 | 0.1 | 0.1 |
| BBP | 0.1 | 0.1 | 0.1 | 0.1 |
| PVB | 0.1 | 0.1 | 0.1 | 0.1 |

YSZ, yttria-stabilized zirconia; LSM, strontium-doped lanthanum manganate; PAG, polyalkalyne glycol; BBP, butyl benzyl phthalate; PVB, polyvinyl butyral.

the case of the single component inks (YSZ, LSM), the ink retained a visually stable suspension for period 2–3 weeks. The cartridges containing these inks were observed to produce stable jets for longer than 2–3 weeks suggesting reasonably stable suspension properties, as excess flocculation or sedimentation in the ink is likely to result in clogging of the print head. In the case of the composite inks (anode interlayer, cathode interlayer), the shelf life of the anode interlayer was about 3–4 weeks, while the cathode interlayer ink required periodic homogenizing.

Figure 1 shows the viscosity of the inks measured at room temperature as well as at printing temperatures (48°C, 58°C) as a function of shear rate. The room temperature viscosity for all inks, both composite and single component inks, exhibit nearly Newtonian behavior over the range of shear rates studied (100–1500 $s^{-1}$). The viscosity values range from 0.058 to 0.063 Pa · s. At the printing temperature (48°C) for single component inks, the viscosity changes from 0.010 to 0.014 Pa · s as the shear rate increases. At printing temperature (58°C) for composite inks, the viscosity changes from 0.006 to 0.012 Pa · s as the shear rate increases. The change in viscosity at higher shear rates (> 800 $s^{-1}$) implies dilatant behavior. On examination of the viscosity curves, it appears that the observed shear thickening behavior is a property of the α-terpineol solvent at elevated temperatures and not brought on by the addition of the binder/plasticizer constituents or solid particles. Even with this shear thickening, though, the viscosities of the inks at elevated temperatures is well below the observed values at room temperature.

### *(2) Cell Microstructure, Performance, and Impedance of Printed Cells*

Figures 2(a) and (b) show the scanning electron microscopy (SEM) cross-sectional view of the two anode supports used for this study. In Fig. 2(a), large flat pores can be seen interspersed through the matrix of the anode body, whereas, equi-axial porosity is seen in Fig. 2(b). Other than the difference in the type of pore former, and hence the type of porosity in the anode support, the two were identical. Only a minor performance improvement was observed for the sample prepared using the substrate with equi-axial pores (type-B). The difference in the back scattering coefficient of YSZ and Ni phases at low acceleration voltage (2 kV, in the present case) results in a contrast in the image, making it possible to distinguish between the two phases.[28] The brighter regions contain Ni, while the darker regions contain YSZ. Type-B anode support was used for most of the study, following the initial characterization of anode supports. Figures 3(a) and (b) show the *V–I* curves of two identical cells, A1-PS (A1—cell 1 with type-A anode support and PS signifies a pasted cathode interlayer and cathode current collection layer) and A2-PS (A2—cell 2 with type-A anode support and PS signifies a pasted cathode interlayer layer and cathode current collection layer). Open circuit voltages were observed to range from 1.12 to 1.16 V, depending on the temperature. As temperature increased from 650° to 850°C, the current density and power density were observed to increase, as well, due to an increase in ionic conductivity of the electrolyte and improved cathode performance at higher temperatures. The maximum power density at 850°C ranged from 0.40 to 0.42 W/$cm^2$. Figures 4(a) and (b) show the SEM cross-sectional views of cell A1-PS and cell A2-PS, respectively, after electrochemical testing. The microstructures of the two cells are identical, reflecting the high reproducibility of printed components. A dense electrolyte of ~10 μm in thickness can be seen with part of the porous cathode below. Above the electrolyte layer, the anode interlayer of ~4–5 μm in thickness can be seen, as well. However, no clear distinction can be seen between the anode support and the anode interlayer. Perhaps this is due to the fact that the composition of the support (55/45 wt% NiO/YSZ) and the anode interlayer (50/50 wt% NiO/YSZ) are similar and hence the transition in porosity between these components very gradual. This apparent similarity between the anode layers could also be due to under-optimized ink formulations. Figures 4(c) and (d) show the top view of the electrolyte portion, not covered by the cath-

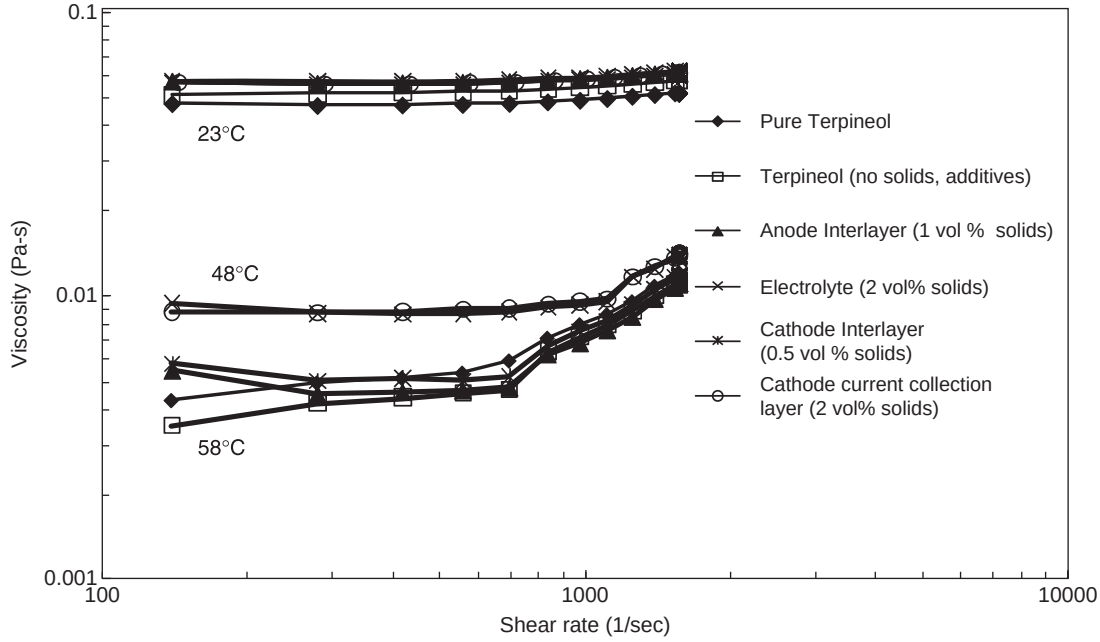


**Fig. 1.** Viscosity of inks as a function of shear rate at room temperature and printing temperatures (48°C, 58°C).

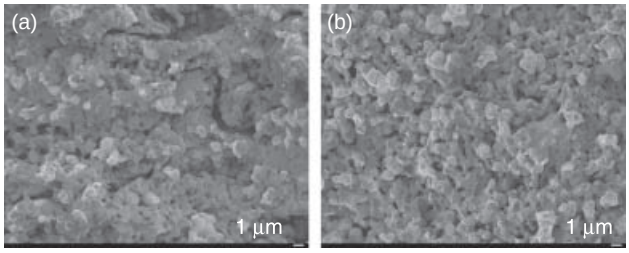


**Fig. 2.** Scanning electron microscopic cross-sectional view: (a) type-A anode support and (b) type-B anode support.

ode, of cells A1-PS and A2-PS. The electrolyte surface is dense, with grains 0.5–1 μm in size, and few blind holes are seen. Similar results were observed for cells prepared using a type-B support. In order to determine the optimal cosintering temperature for the anode-electrolyte layers with respect to electrochemical performance, sintering experiments were carried out in the range of 1350°–1450°C. Figure 5 shows the *V–I* curves for cells B1-PS, B2-PS, and B3-PS whose anode electrolytes were sintered at temperatures of 1350°, 1400°, and 1450°C, respectively. These cells were fabricated on a type-B anode support. They have a printed anode interlayer and electrolyte and pasted cathode interlayer layer and cathode layer. The overall electrochemical performance cells B1-PS and B2-PS are similar in terms of current and power density at temperatures from 650° to 800°C. At 850°C, the maximum power density of B2-PS is 0.5 W/cm$^2$ whereas the maximum power density of B1-PS is 0.46 W/cm$^2$. The current density and power density for cell B3-PS is lower than both B1-PS and B2-PS at all temperatures from 650° to 850°C. From these results it appears that 1400°C is an optimum cosintering temperature. Figures 6(a)–(c) show scanning electron micrograph views of the surface of the electrolyte of the cells B1-PS, B2-PS, and B3-PS. At all cosintering temperatures, the electrolyte is seen to be dense and well sintered. As the cosintering temperature is increased from 1350° to 1450°C, the YSZ grain size is observed to increase from approximately 1–8 μm.

In order to study the impact on cell performance when all components (besides the anode support) are ink-jet printed,

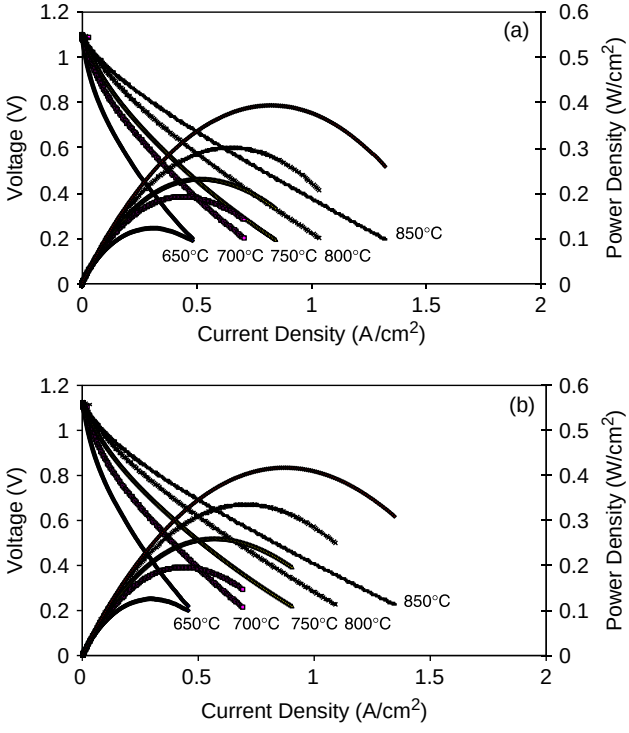


**Fig. 3.** *V–I* curves of two identical cells, (a) A1-PS and (b) A2-PS (A signifies type-A anode support and PS signifies pasted cathode layers).

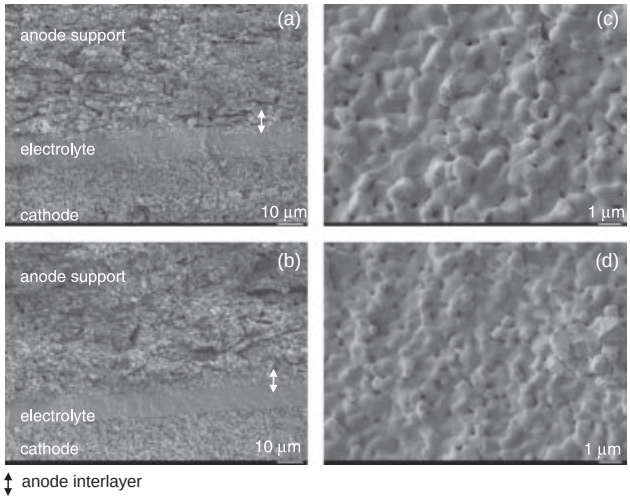


**Fig. 4.** Scanning electron microscopic cross-sectional view of (a) cell, A1-PS; (b) cell, A2-PS; and top view of the electrolyte of (c) cell, A1-PS; (d) cell, A2-PS.

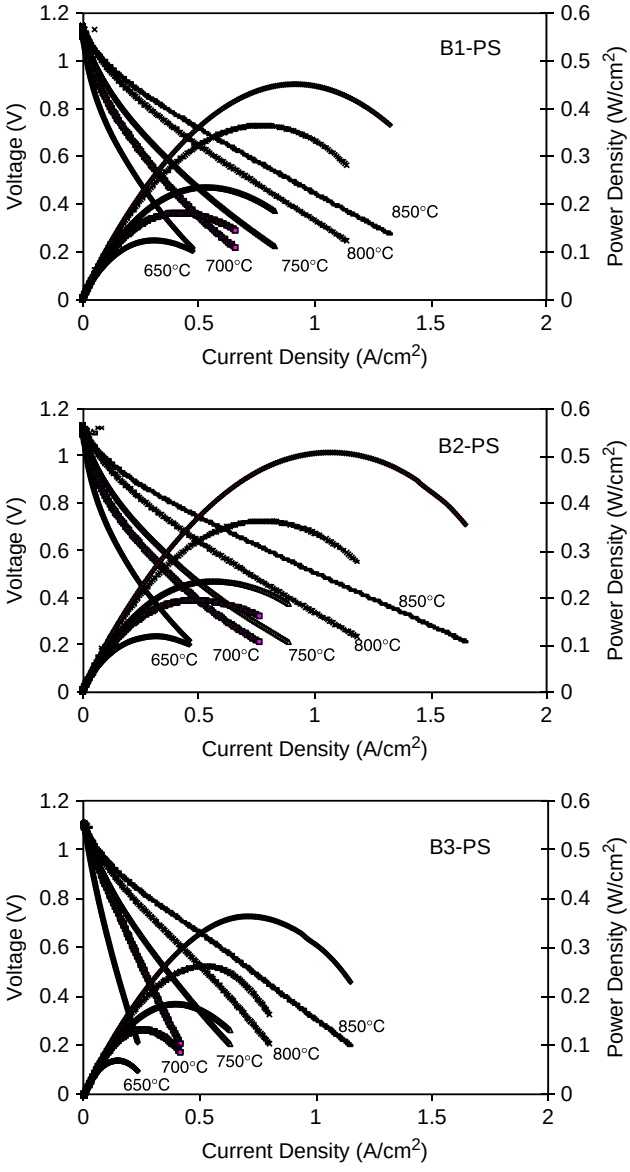


**Fig. 5.** *V–I* curves for cells B1-PS, B2-PS, and B3-PS with anode-electrolytes sintering temperatures of 1350°, 1400°, and 1450°C, respectively (B signifies type-B anode support).

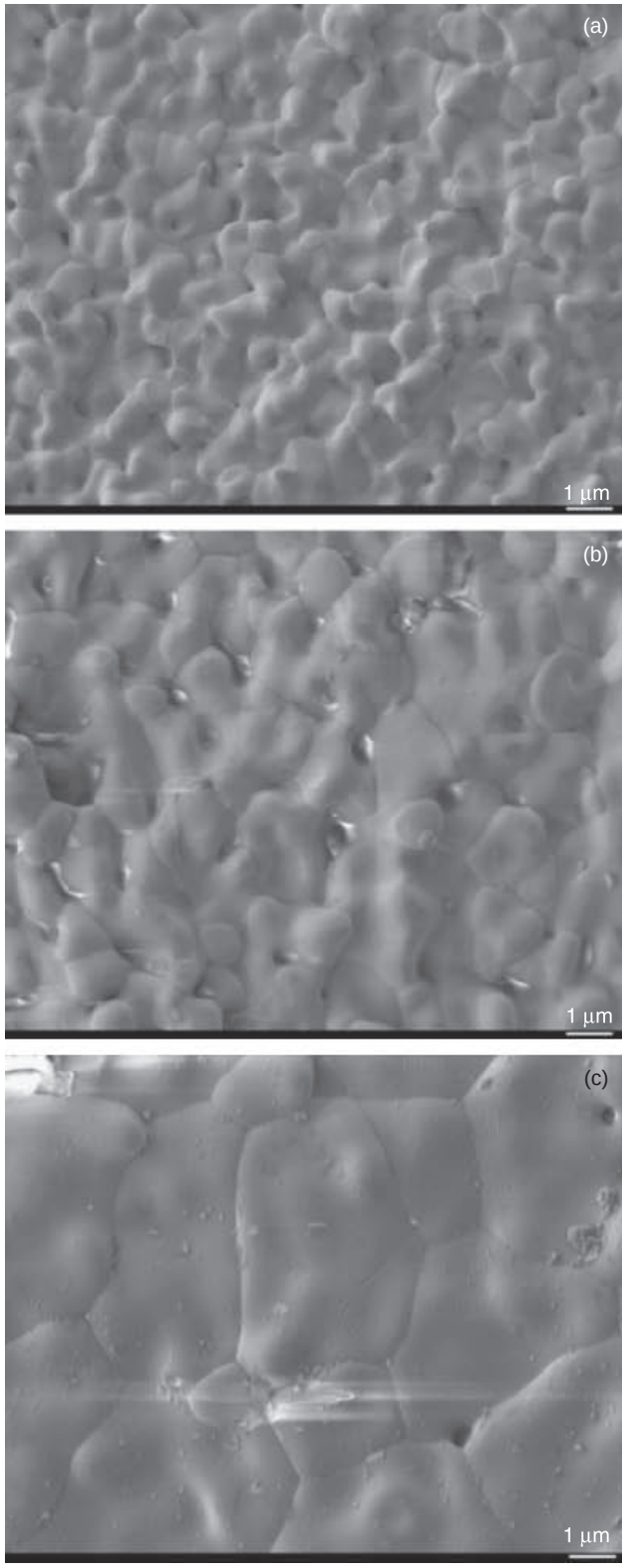


**Fig. 6.** Scanning electron microscopic of the surface of the electrolyte of cells: (a) B1-PS, (b) B2-PS, and (c) B3-PS.

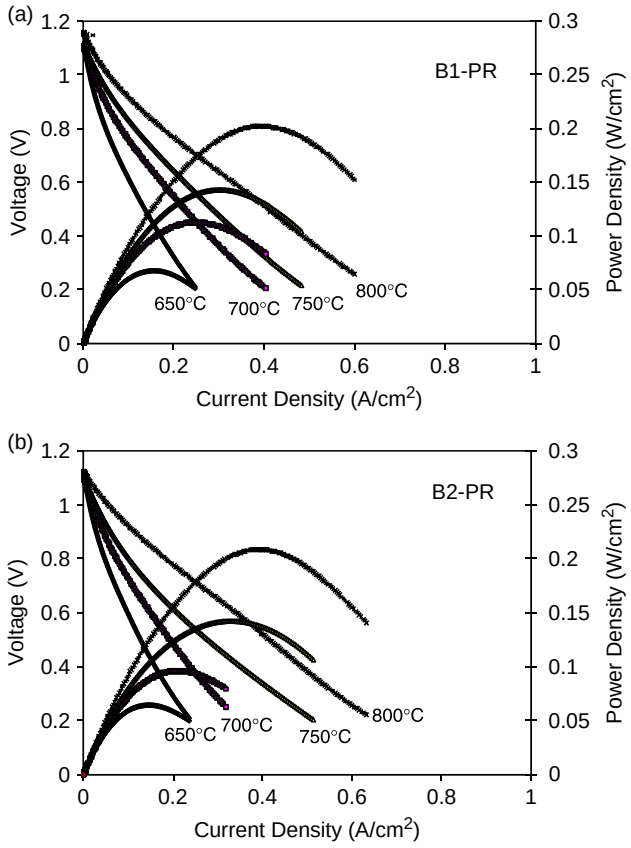


**Fig. 7.** *V–I* curves for two identical cells: (a) B1-PR and (b) B2-PR (PR signifies printed cathode).

electrochemical evaluation was carried out on cells with a printed anode interlayer, electrolyte, cathode interlayer, and cathode current collection layer. These results are shown in Fig. 7 for two identical cells, B1-PR and B2-PR, in the temperature range from 650° to 800°C. For these cells, a type-B anode substrate was used. The printed electrolyte and anode interlayer deposition (12 passes for the electrolyte layer and 10 passes for anode interlayer) was similar to cells B1-PS, B2-PS, and B3-PS. The cosintering temperature of the anode/electrolyte was 1400°C, which was identical to cells B2-PS, A1-PS, and A2-PS. The major difference in cells B1-PR and B2-PR compared with the other cells is that the cathode interlayer and cathode current collecting layers were ink-jet printed rather than hand pasted. In cells B1-PR and B2-PR all supported components (electrolyte, anode functional layer, cathode interlayer layer, and cathode layer) were prepared through the ink-jet approach. A current density of 600 A/cm$^2$ was observed at 800°C for both cells during the polarization study, with a maximum power density of 0.21 W/cm$^2$. Although the performance was not equivalent to that of the pasted cathode cells, very good reproducibility was observed, which can be attributed to the reproducible microstructures afforded through ink-jet deposition. It is assumed that the lower performance observed in the cells produced with ink-jet deposited cathodes was due to an unoptimal cathode microstructure, because all other features were identical to that of B-PS cells. Figure 8 compares the cathode microstructure of a typical pasted cathode cell [(a) B-PS] with that of a printed cathode cell [(b) B-PR]. As observed from Fig. 8, the anode (bottom layer) and electrolyte layers are similar in both images. Over the dense electrolyte layer, the cathode interlayer/cathode region can be seen. In the micrograph of B-PS, two porosity regions can be distinguished, including: a 16-μm-thick cathode interlayer region and a much thicker secondary region composed of pure LSM. The cathode interlayer is composed of a 50/50 wt% LSM/YSZ and is more microporous than the pure LSM layer. No distinction in porosity is observed in the micrograph of B-PR, where the layer was produced through sequential deposition of 20 passes of LSM/YSZ followed by 30 passes of LSM with a 1200°C firing step between the deposition of the two layers. Furthermore, no clear distinction between the layers was observable. Instead, the composite cathode appears to be one continuous layer with no clear definition between the cathode active and current collector regions. More work is necessary to correlate ink properties and deposition parameters

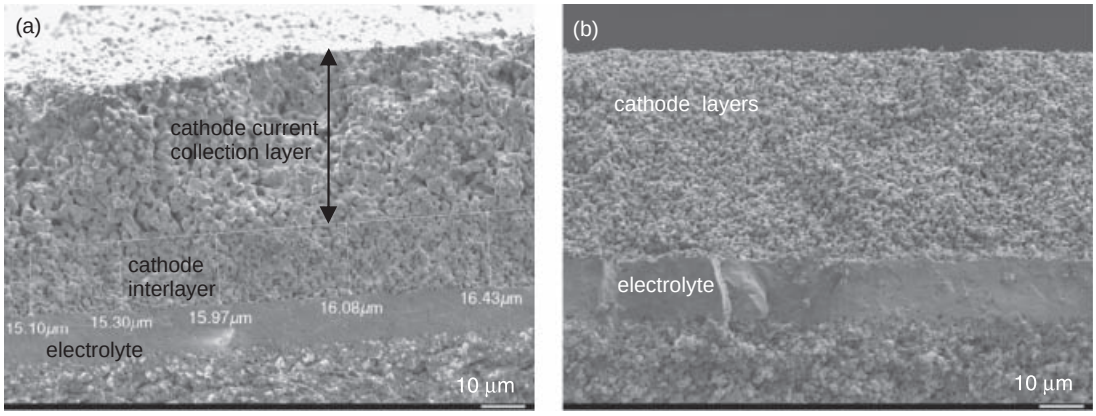


**Fig. 8.** Scanning electron microscopic cross-sectional view of cells: (a) B-PS and (b) B-PR.

with the layer microstructure and its impact on cell performance. One important difference between the pasted and printed cathode layers is the difference in viscosity of the precursor paste and printing ink, respectively. The currently used ink for printing have a low viscosity (0.006–0.012 Pa · s at printing temperatures, as can be seen in Fig. 1) compared with the inks formulated for hand painting (typically 1–5 Pa · s for commercial LSM inks at low shear rates). The cathode microstructure can be controlled by either changing the printing parameters and/or changing the composition of the ink such as solids loading.

Figure 9 shows the impedance plots, under open circuit conditions, at different operating temperatures, for a typical B-PR (printed) and B-PS (pasted) cell with an anode/electrolyte cosintering temperature of 1400°C. The trends in impedance shown in Fig. 9 illustrate both a larger serial resistance ($R_\Omega$ = intercept on the real axis at high frequency) and larger polarization resistance ($R_p$ = the difference in intercept between low and high frequency) for the printed cathode cells compared with the pasted cathode cells at all temperatures. This substantiates the better cell performance for pasted cathode cells compared with printed cathode cells, which was observed. The decrease in overall impedance for both pasted and printed cathode cells, with increasing temperature is due to the increased ionic conductivity of the electrolyte and decreased activation barrier of the cathode. Based on these results, it is clear that further improvement in printing of the cathode layers is required and will be the subject of future research.

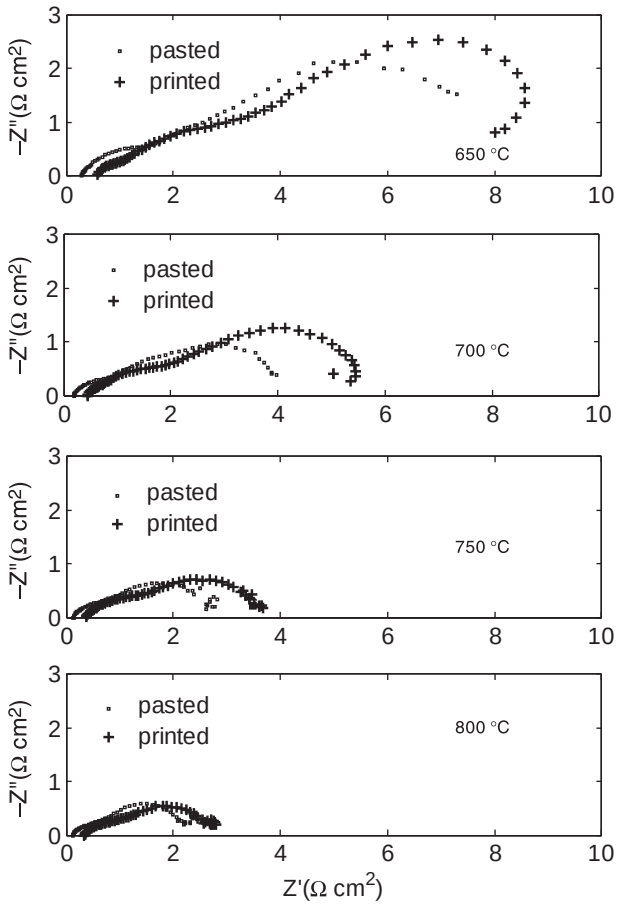


**Fig. 9.** Comparison of impedance (at open circuit conditions) for a typical B-PR and B-PS cell at different temperatures.

## IV. Conclusions

In this work, ink-jet printing has been successfully used to fabricate complete SOFC button cells comprised of electrolyte, anode functional, cathode functional, and cathode current collector layers. SEM of the printed layers revealed a dense electrolyte and porous anode interlayer. Cells tested in hydrogen produced a stable voltage of 1.1 V. Cells incorporating a printed anode interlayer, electrolyte but pasted cathode exhibited a maximum power density of 0.30 W/cm$^2$ at 800°C. Cells comprised of all layers ink-jet printed exhibited slightly lower performance with 0.21 W/cm$^2$ at 800°C. The microstructure of a printed cathode was seen to have tighter pores than a pasted cathode. Additionally, no clear interface was observable between the cathode interlayer and cathode current collection layers for the printed cathode. The impedance of the cell with the printed cathode showed a corresponding increase in ohmic and polarization resistances compared with cells with pasted cathodes. While the current work highlights good reproducibility of cells incorporating ink-jet printed layers, the performance limitations suggest additional optimization of the inks, printing parameters, and firing processes are required before the benefits of this processing approach are fully realized.

## Acknowledgments

The authors wish to acknowledge the help of Mr. Thomas Jenkins with materials processing and cell fabrication and Dr. Allen Jackson for his assistance with the microscopy work.

## References

[1]N. Q. Minh, "Ceramic Fuel Cells," *J. Am. Ceram. Soc.*, **76** [3] 563–88 (1993).
[2]S. Singhal, "Advances in Solid Oxide Fuel Cell Technology," *Solid State Ionics*, **135** [1–4] 305–13 (2000).
[3]B. C. H. Steele, "Materials for IT-SOFC Stacks 35 Years R&D: The Inevitability of Gradualness," *Solid State Ionics*, **134**, 3–20 (2000).
[4]J. W. Fergus, "Electrolytes for Solid Oxide Fuel Cells," *J. Power Sources*, **162**, 30–40 (2006).
[5]P. Holtappels and C. Bagger, "Fabrication and Performance of Advanced Multi-Layer SOFC Cathodes," *J. Eur. Ceram. Soc.*, **22**, 41–8 (2002).

[6]P. Holtappels, C. Sorof, M. C. Verbraeken, S. Rambert, and U. Vogt, "Preparation of Porosity-Graded SOFC Anode Substrates," *Fuel Cells*, **6**, 113–6 (2006).

[7]T. Kenjo and M. Nishiya, "$LaMnO_3$ Air Cathodes Containing $ZrO_2$ Electrolyte for High-Temperature Solid Oxide Fuel-Cells," *Solid State Ionics*, **57**, 295–302 (1992).

[8]T. Kenjo, S. Osawa, and K. Fujikawa, "High-Temperature Air Cathodes Containing Ion Conductive Oxides," *J. Electrochem. Soc.*, **138**, 349–55 (1991).

[9]Y. Lin and S. Barnett, "Co-Firing of Anode-Supported SOFCs with Thin $La_{0.9}Sr_{0.1}Ga_{0.8}Mg_{0.2}O_{3-\delta}$ Electrolytes," *Electrochem. Solid State Lett.*, **9** [6] A285–8 (2006).

[10]A. J. Markworth, K. Ramesh, and W. P. Jr. Parks, "Modeling Studies Applied to Functionally Graded Materials," *J. Mater. Sci.*, **30**, 2183–93 (1995).

[11]T. S. Lai and S. A. Barnett, "Design Considerations for Segmented-In-Series Fuel Cells," *J. Power Sources*, **147**, 85–94 (2005).

[12]M. R. Pillai, D. Gostovic, I. Kim, and S. Barnett, "Effect of Cathode Sheet Resistance on Segmented-In-Series SOFC Power Density," *J. Power Sources*, **163**, 960–5 (2007).

[13]J. Will, A. Mitterdofer, C. Kleinlogel, D. Perednis, and L. J. Gauckler, "Fabrication of Thin Electrolytes for Second-Generation Solid Oxide Fuel Cells," *Solid State Ionics*, **131**, 79–96 (2000).

[14]T. W. Kueper, S. J. Visco, and L. C. De Jonghe, "Thin-Film Ceramic Electrolytes Deposited on Porous and Nonporous Substrates by Sol–Gel Techniques," *Solid State Ionics*, **52**, 251–9 (1992).

[15]A. Negishi, K. Nozaki, and T. Ozawa, "Thin-Film Technology for Solid Electrolyte Fuel-Cells by the rf Sputtering Technique," *Solid State Ionics*, **3/4**, 443–6 (1981).

[16]S. J. Visco, L.-S. Wang, S. Souza, and L. C. De Jonghe, *Mater. Res. Soc. Symp. Proc.*, **369**, 683 (1995).

[17]L. R. Pederson, P. Singh, and X.-D. Zhou, "Application of Vacuum Deposition Methods to Solid Oxide Fuel Cells," *Vacuum*, **80**, 1066–83 (2006).

[18]R. Henne, "Solid Oxide Fuel Cells: A Challenge for Plasma Deposition Processes," *J. Therm. Spray Technol.*, **16** [3] 381–403 (2007).

[19]R. C. Pullar, Y. Zhang, L. F. Chen, S. F. Yang, J. R. G. Evans, P. K. Petrov, A. N. Salak, D. A. Kiselev, A. L. Kholkin, V. M. Fereira, and N. M. Alford, "Manufacture and Measurement of Combinatorial Libraries of Dielectric Ceramics—Part II. Dielectric Measurements of $Ba_{1-x}Sr_xTiO_3$ Libraries," *J. Eur. Ceram. Soc.*, **27** [16] 4437–43 (2007).

[20]T. M. Wang and B. Derby, "Ink-Jet Printing and Sintering of PZT," *J. Am. Ceram. Soc.*, **88** [8] 2053–8 (2005).

[21]X. Zhao, J. R. G. Evans, M. J. Edirisinghe, and J. H. Song, "Ink-Jet Printing of Ceramic Pillar Arrays," *J. Mater. Sci.*, **37** [10] 1987–92 (2002).

[22]C. Ainsley, N. Reis, and B. Derby, "Freeform Fabrication by Controlled Droplet Deposition of Powder Filled Melts," *J. Mater. Sci.*, **37** [15] 3155–61 (2002).

[23]M. Mott and J. R. G. Evans, "Zirconia/Alumina Functionally Graded Material Made by Ceramic Ink-Jet Printing," *Mater. Sci. Eng. A*, **271**, 344–52 (1999).

[24]T. Kawase, S. Moriya, C. J. Newsome, and T. Shimoda, "Ink-Jet Printing of Polymeric Field-Effect Transistors and its Applications," *Jpn. J. Appl. Phys.*, **44** [6] A3649–58 (2005).

[25]T. Xu, S. Petridou, E. H. Lee, E. A. Roth, N. R. Vyavahare, J. J. Hickman, and T. Boland, "Construction of High-Density Bacterial Colony Arrays and Patterns by the Ink-Jet Method," *Biotechnol. Bioneng.*, **85**, 29–33 (2004).

[26]D. Young, A. M. Sukeshini, R. Cummins, H. Xiao, M. Rottmayer, and T. Reitz, "Ink-Jet Printing of Electrolyte and Anode Functional Layer for Solid Oxide Fuel Cells," *J. Power Sources*, **184** [1] 191–6 (2008).

[27]A. M. El-Toni, T. Yamaguchi, S. Shimizu, Y. Fujishiro, and M. Awano, "Development of a Dense Electrolyte Thin Film by the Ink-Jet Printing Technique for a Porous LSM Substrate," *J. Am. Ceram. Soc.*, **91**, 346–9 (2008).

[28]K. Thydén, Y. L. Liu, and J. B. Bilde-Sørensen, "Microstructural Characterization of SOFC Ni–YSZ Anode Composites by Low-Voltage Scanning Electron Microscopy," *Solid State Ionics*, **178**, 1984–9 (2008). □